PIER C

(Received 16 May 2024, Accepted 2 July 2024, Scheduled 29 July 2024)

Modified Adaptive RFT with Sample Covariance Matrix Inversion Recursive Estimation

Haibo Wang*, Wenhua Huang, Haichuang Zhang, Tao Ba, and Zhiqiang Yang

Science and Technology on High Power Microwave Laboratory, Northwest Institute of Nuclear Technology, Xian 710024, China

ABSTRACT: Radon-Fourier transform (RFT) is able to effectively overcome the coupling between the range cell migration (RCM) effect and Doppler modulation by searching along range and velocity dimensions jointly for the moving target, which depends on envelope alignment and Doppler phase compensation. However, without effective clutter suppression, clutter would also be intergraded via RFT. Thus, adaptive RFT (ARFT) has been proposed to clutter suppression by introducing an optimal filter weight, which is determined from the clutter's covariance matrix as well as the steering vector. Nevertheless, the ARFT needs to address the difficulty for real implementation, i.e., computational complexity is too high to a large number of pulse samples. It is known that to obtain the inversion the sample covariance matrix ($\widehat{\mathbf{R}}_{\text{cn}}^{-1}$) is order M^3, i.e., $O(M^3)$, which is the most complexity consumed step in ARFT. In this paper, we propose a modified adaptive RFT (MARFT) method to obtain $\widehat{\mathbf{R}}_{\text{cn}}^{-1}$ with recursive calculation, which takes the complexity order M^2, i.e., $O(M^2)$. Simulations show that the proposed method has the same clutter suppression ability as the conventional ARFT method, while the computational complexity is much lower.

NOMENCLATURE

c	Speed of light
f_c	Center frequency of radar
f_d	Doppler frequency
λ	Wavelength
B	Signal bandwidth
m	Slow time index, $m = 0, 1, \ldots, M-1$
M	Pulse number for integration
T_{r}	Pulse repetition interval
f_{PRF}	Pulse repletion frequency, where $f_{\text{PRF}} = 1/T_r$
t_m	Slow time of radar, where $t_m = mT_r$
τ	Fast time of radar
n	Range cell index
$S_m(\tau)$	Point target echo signal
$Z_m(\tau)$	Received signal in radar system
$\mathbf{Z}$	Received data matrix (digitally sampled $Z_m(\tau)$)
$\text{PSF}(\tau)$	Point target spread function
A_T	Target echoes amplitude after pulse compression
$\otimes$	Convolution operator
$\delta(\cdot)$	The delta function
$(\cdot)^{\text{H}}$	The conjugate transpose
$\mathbf{R}_{\text{cn}}$	$M \times M$-dimensional covariance matrix of clutter plus noise
$\widehat{\mathbf{R}}_{\text{cn}}$	$M \times M$-dimensional sample covariance matrix of clutter plus noise
Δt	Digital sample interval
Δr	Length of range cell
Δv	Length of velocity cell
$\text{round}(\cdot)$	Rounding to integer operator
$G_{\text{RFT}}(\cdot,\cdot)$	Radon-Fourier transform
$G_{\text{ARFT}}(\cdot,\cdot)$	Adaptive Radon-Fourier transform
N_v	Number of cells in velocity searching list
N_r	Number of cells in range search list
$\mathbf{Z}$	Received data matrix
$\mathbf{Z_P}$	Received data matrix int the primary dataset
$\mathbf{Z_R}$	Received data matrix int the reference dataset
C_{P}	The range cell set of Primary data
C_{R}	The range cell set of reference data
C_{R1}	The range cell set of the first part C_{R}
C_{R2}	The range cell set of the second part C_{R}
C_{A}	The range cell set of that may be affected
n_{pARFT}	Pointer to the range cell under ARFT
n_{ps_0}	Pointer to the start of C_{P}
n_{pe_0}	Pointer to the end of C_{P}
n_{ps_1}	Pointer to the start of C_{R1}
n_{pe_1}	Pointer to the end of C_{R1}
n_{ps_2}	Pointer to the start of C_{R2}
n_{pe_2}	Pointer to the end of C_{R2}
n_{ps_3}	Pointer to the start of C_{A}
n_{pe_3}	Pointer to the end of C_{A}
$N_{C_{\text{R}}}$	Number of range cell in C_{R}

* Corresponding author: Haibo Wang (xmuwhb@163.com).

1. INTRODUCTION

Pulse integration for moving targets can improve target detection performance under the condition of noise and clutter. Moving target detection (MTD) method has been widely utilized in the coherent radar system. Both pulse integration and MTD can be efficiently implemented by fast Fourier transform (FFT) in the slow time domain [1]. However, the motion of the target may involve range cell migration (RCM) effect, which results in performance loss for the coherent integration.

Traditional coherent radar signal processing generally adopts the cascaded processing method of pulse compression and Radon-Fourier transform (RFT) [2–5], which can effectively overcome the coupling between the RCM and Doppler modulation by jointly searching along range and velocity dimension

for moving target. Doppler filter banks are also used for the successive integration. Also, generalized RFT is proposed to resolve the higher order polynomial motion in the range dimension [6–10]. Furthermore, wideband scaled RFT is introduced by Qian et al. [11] to resolve echo signal integration for fast moving targets in wideband radar, with noticeable scale effect.

In [12], adaptive Radon-Fourier transform (ARFT) has been proposed to clutter suppression by introducing an optimal filter weight, which is determined from covariance matrix of clutter and noise $\mathbf{R}_{\text{cn}}$ as well as steering vector. For the moving target, it takes the RCM effect in consideration. As to real implementation, ARFT should overcome two difficulties [12]. One is the lack of independently and identically distributed (i.i.d.) training samples in a heterogeneous clutter background. The other is that the computational complexity is too high due to the large number of pulse samples. In conventional ARFT, the sample covariance matrix $\widehat{\mathbf{R}}_{\text{cn}}$ is built by reference data set for each range cell, then $\widehat{\mathbf{R}}_{\text{cn}}^{-1}$ to obtain the optimal filter coefficient by matrix inversion. It takes the computational complexity order M^3, i.e., $O(M^3)$, in which M is the order of the matrix. What make things worse is that the sample covariance matrix should be updated according to the range cell. In this paper, we propose a novel method to calculate $\widehat{\mathbf{R}}_{\text{cn}}^{-1}$ with recursive computation, which takes the complexity order M^2, i.e., $O(M^2)$.

The rest of this paper is organized as follows. In Section 2, the signal model is presented. In Section 3, the modified ARFT method is proposed. The simulation result validates the proposed method in Section 4. Finally, we give some conclusion in Section 6.

2. SIGNAL MODEL OF ARFT

Suppose that there is a target at range r_0, with velocity of v_0, thus

$$r(t) = r(t_m + \tau) \approx r(t_m) = r_0 - v_0 t_m \tag{1}$$

τ is the fast time for radar. And, it starts at t_m, thus $\tau = t - t_m$, which is the slow time for radar. The approximate processing in (1) means that for radar, only the Doppler effect generated by the target's motion needs to be considered in a slow time. The positive direction of velocity is defined as moving toward to the radar. And, m is the slow time index of radar. Taking fixed pulse repetition frequency (PRF) radar for example, t_m can be defined as $t_m = mT_r$ ($m = 0, 1, \ldots, M-1$), where T_r denotes the pulse repletion interval. After pulse compression (PC), the echo signal can be expressed as

$$S_m(\tau) = \text{PSF}\left(\tau - \frac{2r(t_m)}{c}\right) \exp\left(-\text{j}\frac{4\pi f_c r(t_m)}{c}\right) \tag{2}$$

where f_c is the center frequency of radar signal. c is the light speed. $\text{PSF}(\tau)$ denotes the point target spreading function, whose duration is the range resolution, namely $\frac{c}{2B_s}$ where B_s is the bandwidth of transmitting signal. Taking linear frequency modulated (LFM) signal for example, $\text{PSF}(\tau)$ is

$$\text{PSF}(\tau) = \text{sinc}\left(\pi B_s\left(\tau - \frac{2 * r(t_m)}{c}\right)\right) \tag{3}$$

Considering the thermal noise of the receiver, the target echo signal can be expressed as

$$Z_m(\tau) = A_T S_m(\tau) + n_m(\tau) \tag{4}$$

where A_T means the target echo amplitude after pulse compression. $S_m(\tau)$ denotes the point target echo signal, while $Z_m(\tau)$ denotes the received data in radar. $n_m(\tau)$ is the thermal noise. Depending on envelope alignment and additional Doppler phase compensation, RFT method is able to match with the moving target, which can be denoted as follows:

$$\begin{aligned} G_{\text{RFT}}(r, v) &= G_{\text{RFT}}(\tau, v) \\ &= \sum_{m=0}^{M-1}\left(Z_m(\tau) \otimes \delta\left(\tau + \frac{2vt_m}{c}\right)\right) \exp\left(\text{j}\frac{2vt_m}{\lambda}\right) \end{aligned} \tag{5}$$

λ is the wavelength. τ maintains linear relationship with the target range, that is $r = \frac{c\tau}{2}$. $G_{\text{RFT}}(r, v)$ represents the RFT integration in range and velocity dimension. $\delta(\cdot)$ represents the delta function. '$\otimes$' is the convolution operator. The function of this operator in (5) is to compensate the envelope alignment. $\exp(\text{j}\frac{2vt_m}{\lambda})$ denotes the additional doppler phase compensation.

As for digitally sampled echo signal, the envelope alignment operation is realised by data shifting, accordingly:

$$Z_m(\tau) \otimes \delta\left(\tau + \frac{2vt_m}{c}\right) = \mathbf{Z}(m, n + n_{\text{shift}}(m)) \tag{6}$$

where

$$n_{\text{shift}}(m) = \text{round}\left(\frac{2vt_m}{\Delta r}\right) \tag{7}$$

$\mathbf{Z}$ means the received data matrix, which is digitally sampled $Z_m(\tau)$. The row index of $\mathbf{Z}$ represents the slow time index, $m = 0, 1, 2, \ldots, M-1$. The column index of $\mathbf{Z}$ is the fast time sample number. Δr is the length of range cell, and we have $\Delta r = \frac{c\Delta t}{2}$ where Δt is the digital sample interval in radar. round$(\cdot)$ is the function to find the nearest integer. Thus, as to algorithm actually implemented, (6) can be realized by data shifting or pointer offset.

Apart from noise, there may be clutter in radar echoes, which may seriously affect target detection ability without clutter suppression method. In RFT, in order to get long time coherent integration, both the 'main lobe' and 'side lobe' of strong clutter would affect target detection [12]. Radar ground clutter is assumed to be concentrated at low Doppler frequency normally, as the echoes of those 'targets' are motionless.

In conventional ARFT, the received data are divided into two sets, i.e., the primary dataset and the secondary dataset (reference dataset). The first dataset is assumed to contain target echoes, while the latter dataset is supposed to contain clutter and noise only. Fig. 1 illustrates the datasets in AFT. The optimal filter weight is derived form the clutter's covariance matrix, which is substituted by its maximum-likelihood estimate (MLE), i.e., the sample covariance matrix (SCM) [13, 14], which is calculated echo in reference dataset.

$$G_{\text{ARFT}}(r, v) = \sum_{m=0}^{M-1}\left(\widehat{\mathbf{R}}_{\text{cn}}^{-1}(m, :) \cdot \mathbf{Z}_{\text{P}}(:, n_{\text{pARFT}} + n_{\text{shift}}(m))\right)$$

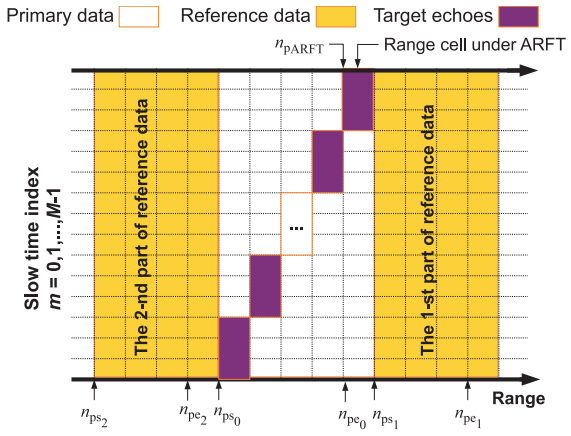

FIGURE 1. Illustration for ARFT.

$$\exp\left(\mathrm{j}\frac{2vt_m}{\lambda}\right) \tag{8}$$

where n_{pARFT} denotes the pointer (index) to the range cell that is under ARFT integration. $\mathbf{Z_P}$ is the received data matrix in the primary dataset,

$$\mathbf{Z}_{\text{P}} = \mathbf{Z}(0 : M-1, C_{\text{P}}) \tag{9}$$

C_{P} denotes the primary range cell set.

$$C_{\text{P}} = \{n | n_{\text{ps}_0} \le n \le n_{\text{pe}_0}\} \tag{10}$$

n_{ps_0} and n_{pe_0} denote the pointers to the start of C_{P} and the end of C_{P}, respectively. $\widehat{\mathbf{R}}_{\text{cn}}^{-1}$ is the inverse of SCM which can be obtained as follows

$$\widehat{\mathbf{R}}_{\text{cn}} = \frac{1}{N_{C_{\text{R}}}}\mathbf{Z}_{\text{R}}\mathbf{Z}_{\text{R}}^{\text{H}} \tag{11}$$

where $\mathbf{Z_R}$ is the received data matrix in the reference dataset.

$$\mathbf{Z}_{\text{R}} = \mathbf{Z}(0 : M-1, C_{\text{R}}) \tag{12}$$

C_{R} is the reference range cell set, which contains two parts, before C_{P} and after C_{P}, respectively, and it is clearly illustrated by Fig. 1.

$$C_{\text{R}} = C_{\text{R1}} \bigcup C_{\text{R2}} \tag{13}$$

$$C_{\text{R1}} = \{n | n_{\text{ps}_1} \le n \le n_{\text{pe}_1}\},$$

$$C_{\text{R2}} = \{n | n_{\text{ps}_2} \le n \le n_{\text{pe}_2}\} \tag{14}$$

n_{ps_1}, n_{pe_1}, n_{ps_2} and n_{pe_2} denote the pointers to the start of C_{R1}, the end of C_{R1}, the start of C_{R2}, and the end of C_{R2}, respectively. $N_{C_{\text{R}}}$ is the number of range cells in C_{R},

$$N_{C_{\text{R}}} = |C_{\text{R}}| = \left(|n_{\text{ps}_1} - n_{\text{pe}_1}| + 1\right) + \left(|n_{\text{ps}_2} - n_{\text{pe}_2}| + 1\right) \tag{15}$$

From Fig. 1, we have

$$n_{\text{ps}_0} = n_{\text{pe}_2} + 1, \quad n_{\text{ps}_1} = n_{\text{pe}_0} + 1 \tag{16}$$

Conventionally, the degree of freedom (DOF) of clutter is lower than the dimension of matrix $\widehat{\mathbf{R}}_{\text{cn}}$, thus $\widehat{\mathbf{R}}_{\text{cn}}$ would be ill-conditioned. Consequently, diagonal loading technic [15] is usually utilized to avoid numerical errors.

$$\widehat{\mathbf{R}}_{\text{cn}} = \frac{1}{N_{C_{\text{R}}}}\mathbf{Z}_{\text{R}}\mathbf{Z}_{\text{R}}^{\text{H}} + \gamma\sigma^2\mathbf{I} \tag{17}$$

where σ^2 is the background noise level. As for a radar receiver which has been carefully calibrated, σ^2 is known. γ is the loading level.

According to the well-known Reed-Malleett-Brennman (RMB) rule proposed in [16], in order to ensure that the signal-to-clutter-pulse-noise ratio (SCNR) improvement factor (IF) loss is less than 3 dB, the number of samples in reference dataset should be at least twice larger than the number of integrated pulses, i.e.,

$$N_{C_{\text{R}}} \ge 2M \tag{18}$$

For conventional ARFT, range cell sets C_{P} and C_{R} are determined by the point of (r, v) in (8). Also, SCM should be recalculated. What makes things worse is that matrix inverse operation should be recalculated repeatedly.

3. SAMPLE COVARIANCE MATRIX INVERSION RECURSIVE ESTIMATION METHOD

SCM should be recalculated as to new point of (r, v) in (8); however, as to the points near each other, the major part of element in dataset C_{R} keeps the same as its former one. Thus, as to the conventional ARFT, much computational complexity in (11) and matrix inversion seems to be wasteful.

In this paper, we propose modified adaptive RFT (MARFT), in which, the dataset configuration is little different from the conventional ARFT. First of all, velocity searching range is prerequisite of the algorithm, i.e., v_{min} and v_{max}. Thus, as to certain range cell (n_{pARFT} pointing at) under ARFT, the range cell set C_{A} that will be affected by the target is determined, which is illustrated by Fig. 2.

$$C_{\text{A}} = \{n | n_{\text{ps}_3} \le n \le n_{\text{pe}_3}\} \tag{19}$$

where n_{ps_3} and n_{pe_3} are the pointers to the start and end of C_{A}, respectively. Thus, as to new velocity for AFT searching, C_{A}

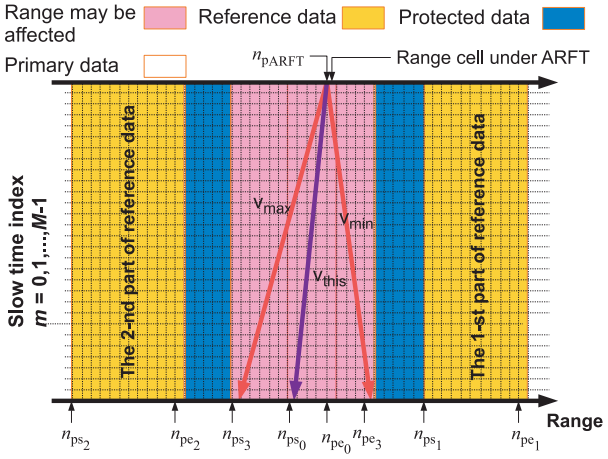

FIGURE 2. Configuration of MARFT.

keeps the same. However, when n_{pARFT} is moving to the next range cell,

$$n_{\text{pARFT}}^{\text{new}} = n_{\text{pARFT}} + 1; \tag{20}$$

C_{A} should be updated accordingly.

$$n_{\text{ps}_3}^{\text{new}} = n_{\text{ps}_3} + 1, \quad n_{\text{pe}_3}^{\text{new}} = n_{\text{pe}_3} + 1 \tag{21}$$

Being different from the conventional ARFT, we set up protected range cell to avoid SCM estimation error, which is a general request in radar target detection, and it can be found in Fig. 2. n_{ps_1}, n_{pe_1}, n_{ps_2}, and n_{pe_2} are also unitized to denote the pointers to the start of C_{R1}, the end of C_{R1}, the start of C_{R2}, and the end of C_{R2}, and they should be updated accordingly.

$$\begin{aligned} n_{\text{ps}_0}^{\text{new}} &= n_{\text{ps}_0} + 1, \quad n_{\text{pe}_0}^{\text{new}} = n_{\text{pe}_0} + 1, \\ n_{\text{ps}_1}^{\text{new}} &= n_{\text{ps}_1} + 1, \quad \text{and } n_{\text{pe}_1}^{\text{new}} = n_{\text{pe}_1} + 1 \end{aligned} \tag{22}$$

It is illustrated by Fig. 3.

$$\begin{aligned} C_{\text{R1}}^{\text{new}} &= \left(C_{\text{R1}} - \{n_{\text{ps}_1}\}\right) \bigcup \{n_{\text{pe}_1}^{\text{new}}\}, \\ C_{\text{R2}}^{\text{new}} &= \left(C_{\text{R2}} - \{n_{\text{ps}_2}\}\right) \bigcup \{n_{\text{pe}_2}^{\text{new}}\} \end{aligned} \tag{23}$$

And,

$$C_{\text{R}}^{\text{new}} = C_{\text{R1}}^{\text{new}} \bigcup C_{\text{R2}}^{\text{new}} \tag{24}$$

Based on (24), it is obvious that $N_{C_{\text{R}}}$ in (15) keeps the same. We use $\mathbf{u}_1$, $\mathbf{u}_2$, $\mathbf{v}_1$, and $\mathbf{v}_2$ to denote the data vector that needs to be removed from C_{R1}, the data vector that needs to be removed from C_{R2}, the data vector that needs to be added into C_{R1}, and the data vector that needs to be added into C_{R2}, respectively. It is illustrated clearly by Fig. 3.

$$\begin{aligned} \mathbf{u}_1 &= \mathbf{Z}(:, n_{\text{ps}_1}), \quad \mathbf{u}_2 = \mathbf{Z}(:, n_{\text{ps}_2}), \\ \mathbf{v}_1 &= \mathbf{Z}(:, n_{\text{pe}_1}^{\text{new}}), \quad \text{and } \mathbf{v}_2 = \mathbf{Z}(:, n_{\text{pe}_2}^{\text{new}}) \end{aligned} \tag{25}$$

Consequently, SCM in both (11) and (17) can be updated by

$$\widehat{\mathbf{R}}_{\text{cn}}^{\text{new}} = \widehat{\mathbf{R}}_{\text{cn}} - \frac{\mathbf{u}_1\mathbf{u}_1^{\text{H}} + \mathbf{u}_2\mathbf{u}_2^{\text{H}}}{N_{C_{\text{R}}}} + \frac{\mathbf{v}_1\mathbf{v}_1^{\text{H}} + \mathbf{v}_2\mathbf{v}_2^{\text{H}}}{N_{C_{\text{R}}}} \tag{26}$$

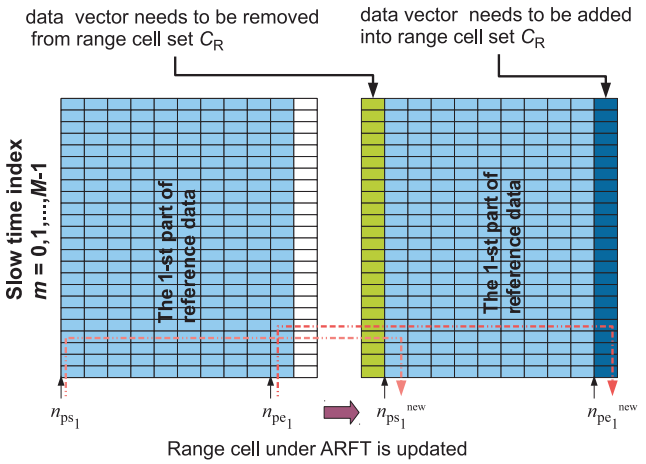

FIGURE 3. Update of reference range cell set.

In (26), some part of new datasets are added into SCM; however some datasets are removed from it. In other words, the major part of SCM keeps the same. Thus, the latest inverse of SCM may be useful.

It is well known of the matrix inverse formula

$$\begin{aligned} \left(\mathbf{A} + \mathbf{s}\mathbf{s}^{\text{H}}\right)^{-1} &= \mathbf{A}^{-1} - \frac{\mathbf{A}^{-1}\mathbf{s}\mathbf{s}^{\text{H}}\mathbf{A}^{-1}}{1 + \mathbf{s}^{\text{H}}\mathbf{A}^{-1}\mathbf{s}}, \\ \left(\mathbf{A} - \mathbf{s}\mathbf{s}^{\text{H}}\right)^{-1} &= \mathbf{A}^{-1} + \frac{\mathbf{A}^{-1}\mathbf{s}\mathbf{s}^{\text{H}}\mathbf{A}^{-1}}{1 - \mathbf{s}^{\text{H}}\mathbf{A}^{-1}\mathbf{s}} \end{aligned} \tag{27}$$

The details of (27) can be found in Appendix A. Thus, the recursive operator is defined as

$$F(\mathbf{A}, \mathbf{z}, \alpha) = \begin{cases} \mathbf{A}^{-1} - \frac{\mathbf{A}^{-1}\mathbf{z}\mathbf{z}^{\text{H}}\mathbf{A}^{-1}}{1+\mathbf{z}^{\text{H}}\mathbf{A}^{-1}\mathbf{z}} & \alpha = 1 \\ \mathbf{A}^{-1} + \frac{\mathbf{A}^{-1}\mathbf{z}\mathbf{z}^{\text{H}}\mathbf{A}^{-1}}{1-\mathbf{z}^{\text{H}}\mathbf{A}^{-1}\mathbf{z}} & \alpha = -1 \end{cases} \tag{28}$$

in which, $\mathbf{A}$ is the major matrix, and $\mathbf{z}$ is the vector that will be added into or remove from $\mathbf{A}^{-1}$.

Based on the C_{R} updating Eq. (24), the inverse of SCM should be updated by 4 steps, which is illustrated by Fig. 4. Fig. 5 shows the detailed process of the entire algorithm.

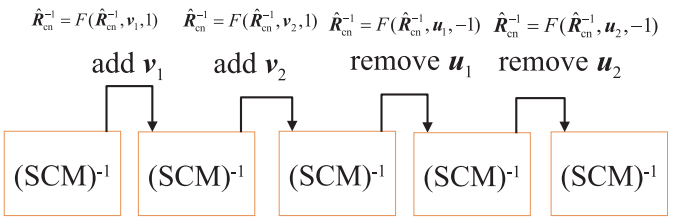

FIGURE 4. Illustration of updating method of the inverse of SCM.

Input: Received data matrix $\mathbf{Z}$;
The range search list:
$\boldsymbol{r} = [r(1), r(2), ..., r(n_r), ..., r(N_r)]$;
The velocity search list:
$\boldsymbol{v} = [v(1), v(2), ..., , ...v(N_v)]$;
Output: Adaptive RFT integration reslut: $G_{\text{ARFT}}(r, v)$
Initialize n_{pARFT};
Initialize C_{A}, C_{R} based on the maximum and minimum value in the velocity search list;
Initialize the pointers: n_{ps1}, n_{pe1}, n_{ps2}, n_{pe2}, $n_{\text{ps3}}$and n_{pe3}
Get the first SCM based on C_{R} by 18)
Get the inversion of SCM
for $n_v = 1, 2, ..., N_v$ **do**
  Get $G_{\text{ARFT}}(n_{\text{pARFT}}, v(n_v))$ by (9)
end
while ***True*** **do**
  $n_{\text{pARFT}} = n_{\text{pARFT}} + 1$;
  Update C_{A}, C_{R};
  Find the vector in (26);
  Update $\hat{\boldsymbol{R}}_{\text{cn}}^{-1}$;
  Update the pointers: : n_{ps1}, n_{pe1}, n_{ps2}, n_{pe2}, $n_{\text{ps3}}$and n_{pe3} by (22) and (23)
  for $n_v = 1, 2, ..., N_v$ **do**
    Get $G_{\text{ARFT}}(n_{\text{pARFT}}, v(n_v))$ by (9)
  end
end

FIGURE 5. ARFT integration with recursive SCM.

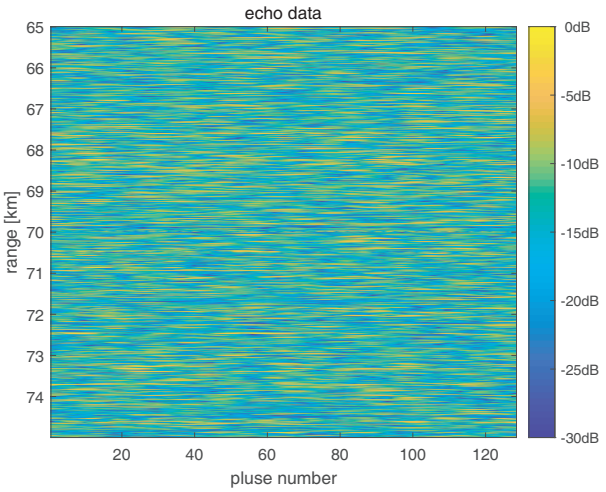

FIGURE 6. Echo data after pulse compression.

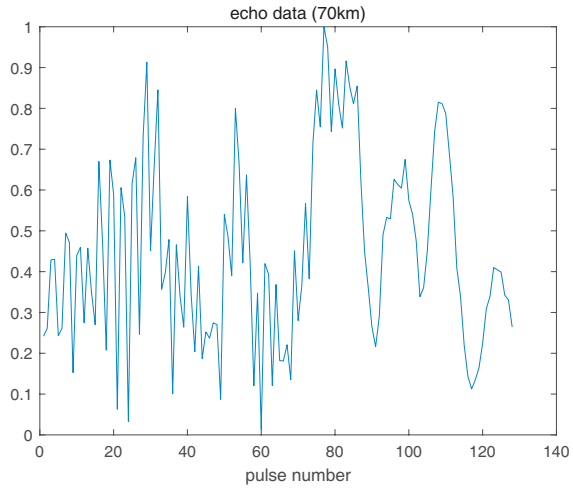

FIGURE 7. Range sclice of Echo data.

4. ANALYSIS OF COMPUTATIONAL COMPLEXITY

In this section, we give the comparison of the computational complexity between the convectional ARFT and MARFT. For the sake of simplicity, we use I_{ac} and I_{mc} to represent the complex addition and complex multiplication, respectively. The computational complexity of RFT is

$$I_{\text{RFT}} = N_r N_v (M I_{mc} + (M-1) I_{ac}) \tag{29}$$

The computational complexity of SCM estimation is

$$I_{\text{SCM}_\text{E}} = N_{C_R} M^2 I_{mc} + N_{C_R} (M-1) I_{ac} \tag{30}$$

The computational complexity of SCM inversion is approximated by

$$I_{\text{SCM}_\text{I}} = M^3 I_{mc}/3 \tag{31}$$

The computational complexity of ARFT integration in (8) for one range cell is

$$I_{\text{cell}} = 2M I_{mc} + (M-1) I_{ac} \tag{32}$$

Thus, the total computational complexity of the conventional ARFT

$$\begin{aligned} I_{\text{ARFT}_\text{C}} &= N_r N_v (I_{\text{SCM}_\text{E}} + I_{\text{SCM}_\text{I}} + I_{\text{cell}}) \\ &= N_r N_v \Big((N_{C_R} M^2 + M^3/3 + 2M) I_{mc} \\ &\quad + (N_{C_R} + 1)(M-1) I_{ac} \Big) \end{aligned} \tag{33}$$

The computational complexity of the SCM recursive operator (28) is

$$I_{\text{SCM}_\text{R}} = (2M^2 + 2M) I_{mc} + (M^2 + 2M - 1) I_{ac} \tag{34}$$

Thus, the total computational complexity of the MARFT

$$\begin{aligned} I_{\text{ARFT}_\text{R}} &= I_{\text{SCM}_\text{E}} + I_{\text{SCM}_\text{I}} + N_v I_{\text{cell}} \\ &\quad + (N_r - 1) N_v (4 I_{\text{SCM}_\text{R}} + I_{\text{cell}}) \end{aligned} \tag{35}$$

Thus,

$$\begin{aligned} I_{\text{ARFT}_\text{R}} &= (N_{C_R} M^2 + M^3/3) I_{mc} + N_{C_R} (M-1) I_{ac} \\ &\quad + N_v \big(2M I_{mc} + (M-1) I_{ac} \big) \\ &\quad + (N_r - 1) N_v \big((8M^2 + 10M) I_{mc} \\ &\quad + (4M^2 + 9M - 2) I_{ac} \big) \end{aligned} \tag{36}$$

The comparison between (33) and (35) shows that SCM recursive method can reduce the computational complexity significantly.

5. NUMERICAL EXPERIMENTS

This section is devoted to evaluating the performance of the proposed method via computer simulations, where the parameters of radar are shown in Table 1, in which SNR and SCR are measured by the echo signal after pulse compression. The code development environment is Octave on a 64 bit Windows 7 operating system, and the computer's CPU is Intel (R) Core (TM) i7-7700@3.6 GHz, installed with 32 GB of system memory.

Figure 6 illustrates the echo data after pulse compression, and Fig. 7 is the range slice of Fig. 6 with 70 km. The echo of target

TABLE 1. Parameters setup in simulation.

Parameter	Value
Carrier frequency (f_c)	5 GHz
Pulse repetition frequency (PRF)	500 Hz
Velocity ambiguity	15 m/s
Range resolution	15 m
Pulse number for integration (M)	128
Target number	2
Target A initial range	70 km
Target A velocity	80 m/s
Target B initial range	69.5 km
Target B velocity	78 m/s
Signal to noise ratio (SNR)	20 dB
Signal to clutter ratio (SCR)	-15 dB and -30 dB
loading level in Eq. (17)	0.01

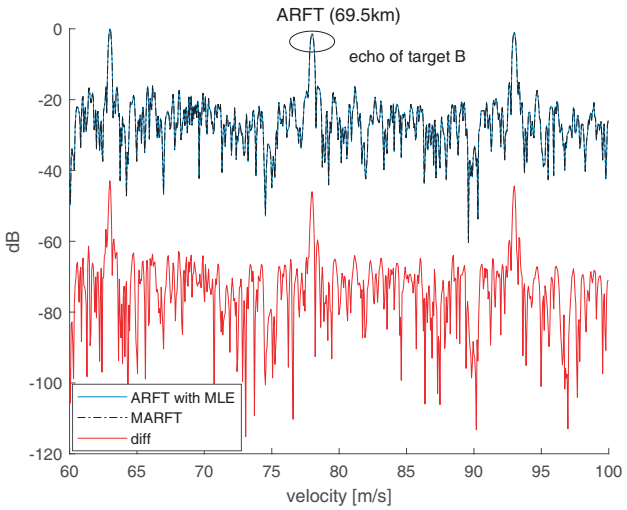

FIGURE 8. ARFT and MARFT results at range 69.5 km (SCR = −15 dB).

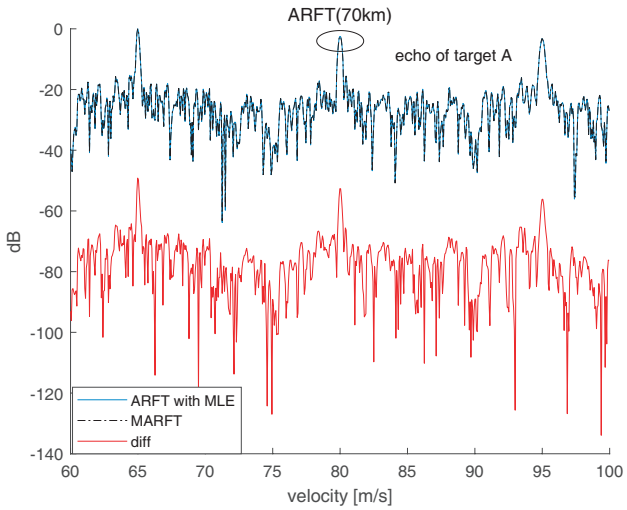

FIGURE 9. ARFT and MARFT results at range 70 km (SCR = −15 dB).

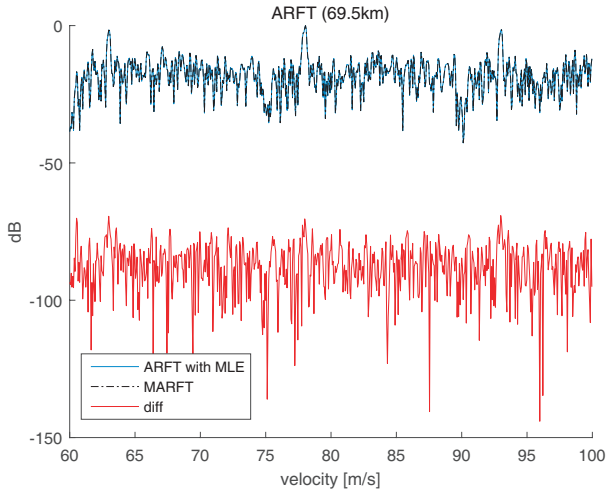

FIGURE 10. ARFT and MARFT results at range 69.5 km (SCR = −30 dB).

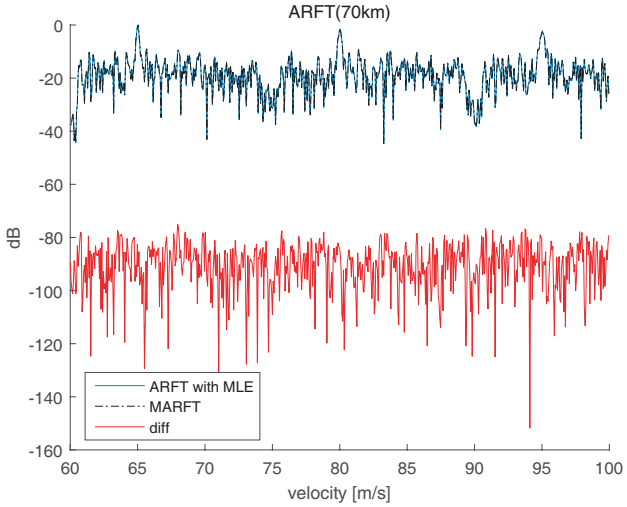

FIGURE 11. ARFT and MARFT results at range 70 km (SCR = −30 dB).

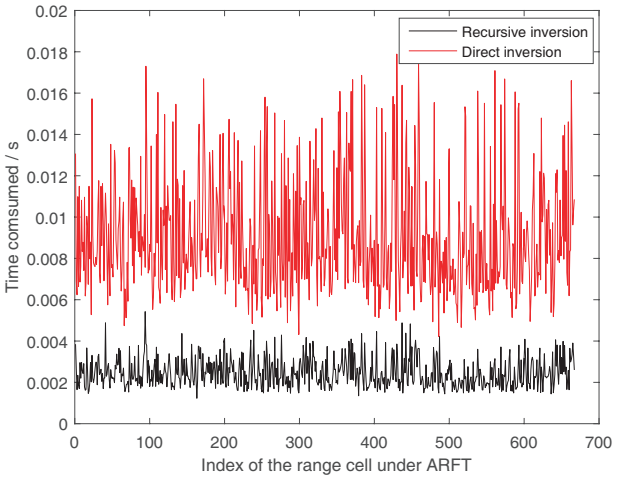

FIGURE 12. Time consumed to obtain the inversion of SCM.

cannot be distinguished in original data, which is obscured in clutter.

ARFT has been applied to suppress clutter, in which SCM is calculated by MLE. Also, MARFT takes effect, in which inverse of SCM is calculated recursively. Fig. 8 and Fig. 9 illustrate the ARFT results at range slice of 69.5 km and 70 km, respectively, as SCR = −15 dB. Also, Fig. 10 and Fig. 11 illustrate the ARFT results at range slice of 69.5 km and 70 km, respectively, as SCR = −30 dB. Both conventional ARFT and MARFT are displayed, as well as the difference of the two methods. According to the simulation results, the difference of numerical results between ARFT and MARFT can be ignored.

Figure 12 shows the time consumed to obtain inversion of SCM, both recursive calculation and directly inversion. It is obvious that recursive calculation takes much less time than directly inversion.

6. CONCLUSION

In this paper, a recursive method to calculate the inversion of a sample covariance matrix $\widehat{\mathbf{R}}_{\text{cn}}$ has been proposed. Theoretical analysis shows that MAFT can reduce the computational complexity significantly. According to the simulation results, the difference between ARFT and MARFT can be ignored.

APPENDIX A. PROOF OF THE MATRIX INVERSE FORMULA

Suppose that there are matrices $\mathbf{A}_{n\times m}$, $\mathbf{B}_{n\times m}$, $\mathbf{C}_{m\times m}$, and $\mathbf{D}_{m\times n}$, the Sherman-Morrison formula is

$$(\mathbf{A}+\mathbf{BCD})^{-1} = \mathbf{A}^{-1}-\mathbf{A}^{-1}\mathbf{B}(\mathbf{DA}^{-1}\mathbf{B}+\mathbf{C}^{-1})^{-1}\mathbf{DA}^{-1} \quad \text{(A1)}$$

Let, $\mathbf{B}=\mathbf{s}$, $\mathbf{C}=1$, $\mathbf{D}=\mathbf{s}^{\text{H}}$, then we have

$$\left(\mathbf{A}+\mathbf{ss}^{\text{H}}\right)^{-1} = \mathbf{A}^{-1} - \frac{\mathbf{A}^{-1}\mathbf{ss}^{\text{H}}\mathbf{A}^{-1}}{1+\mathbf{s}^{\text{H}}\mathbf{A}^{-1}\mathbf{s}} \quad \text{(A2)}$$

Let, $\mathbf{B}=\mathbf{s}$, $\mathbf{C}=-1$, $\mathbf{D}=\mathbf{s}^{\text{H}}$, then we have

$$\left(\mathbf{A}-\mathbf{ss}^{\text{H}}\right)^{-1} = \mathbf{A}^{-1} + \frac{\mathbf{A}^{-1}\mathbf{ss}^{\text{H}}\mathbf{A}^{-1}}{1-\mathbf{s}^{\text{H}}\mathbf{A}^{-1}\mathbf{s}} \quad \text{(A3)}$$

REFERENCES

[1] Aubry, A., A. D. Maio, V. Carotenuto, and A. Farina, "Radar phase noise modeling and effects — Part I: MTI filters," *IEEE Transactions on Aerospace and Electronic Systems*, Vol. 52, No. 2, 698–711, 2016.

[2] Xu, J., J. Yu, Y.-N. Peng, and X.-G. Xia, "Radon-Fourier transform for radar target detection, I: Generalized Doppler filter bank," *IEEE Transactions on Aerospace and Electronic Systems*, Vol. 47, No. 2, 1186–1202, 2011.

[3] Lang, P., X. Fu, J. Dong, and J. Yang, "An efficient Radon-Fourier transform-based coherent integration method for target detection," *IEEE Geoscience and Remote Sensing Letters*, Vol. 20, 1–5, 2023.

[4] Hussain, M., R. Ahmed, and H. M. Cheema, "Segmented Radon-Fourier transform for long time coherent radars," *IEEE Sensors Journal*, Vol. 23, No. 9, 9582–9594, 2023.

[5] Longman, O. and I. Bilik, "Spectral Radon-Fourier transform for automotive radar applications," *IEEE Transactions on Aerospace and Electronic Systems*, Vol. 57, No. 2, 1046–1056, 2021.

[6] Xu, J., X.-G. Xia, S.-B. Peng, J. Yu, Y.-N. Peng, and L.-C. Qian, "Radar maneuvering target motion estimation based on generalized radon-fourier transform," *IEEE Transactions on Signal Processing*, Vol. 60, No. 12, 6190–6201, 2012.

[7] Wu, W., G. H. Wang, and J. P. Sun, "Polynomial Radon-polynomial Fourier transform for near space hypersonic maneuvering target detection," *IEEE Transactions on Aerospace and Electronic Systems*, Vol. 54, No. 3, 1306–1322, 2017.

[8] Qian, L.-C., J. Xu, X.-G. Xia, W.-F. Sun, T. Long, and Y.-N. Peng, "Fast implementation of generalised Radon-Fourier transform for manoeuvring radar target detection," *Electronics Letters*, Vol. 48, No. 22, 1427–1428, 2012.

[9] Zhang, Z., N. Liu, Y. Hou, S. Zhang, and L. Zhang, "A coherent integration segment searching based GRT-GRFT hybrid integration method for arbitrary fluctuating target," *Remote Sensing*, Vol. 14, No. 11, 2695, 2022.

[10] Xu, J., J. Yu, Y.-N. Peng, X.-G. Xia, and T. Long, "Space-time Radon-Fourier transform and applications in radar target detection," *IET Radar, Sonar & Navigation*, Vol. 6, No. 9, 846–857, 2012.

[11] Qian, L.-C., J. Xu, X.-G. Xia, W.-F. Sun, T. Long, and Y.-N. Peng, "Wideband-scaled Radon-Fourier transform for high-speed radar target detection," *IET Radar, Sonar & Navigation*, Vol. 8, No. 5, 501–512, 2014.

[12] Xu, J., L. Yan, X. Zhou, T. Long, X.-G. Xia, Y.-L. Wang, and A. Farina, "Adaptive Radon-Fourier transform for weak radar target detection," *IEEE Transactions on Aerospace and Electronic Systems*, Vol. 54, No. 4, 1641–1663, 2018.

[13] Pillai, S. U., *Array Signal Processing*, Springer-Verlag, 1989.

[14] Guerci, J. R., *Space-Time Adaptive Processing for Radar*, 2nd ed., Artech House, 2015.

[15] Carlson, B. D., "Covariance matrix estimation errors and diagonal loading in adaptive arrays," *IEEE Transactions on Aerospace and Electronic Systems*, Vol. 24, No. 4, 397–401, 1988.

[16] Reed, I. S., J. D. Mallett, and L. E. Brennan, "Rapid convergence rate in adaptive arrays," *IEEE Transactions on Aerospace and Electronic Systems*, Vol. AES-10, No. 6, 853–863, 1974.

Erratum to "Modified Adaptive RFT with Sample Covariance Matrix Inversion Recursive Estimation"

by Haibo Wang, Wenhua Huang, Haichuang Zhang, Tao Ba, and Zhiqiang Yang
in *Progress in Electromagnetic Research C*, Vol. 145, 181–187, 2024

During the proofreading of the manuscript, we discovered an error in the corresponding author's information due to our oversight. The correct corresponding author should be Professor Haichuan Zhang (zhanghai_scholar@163.com); however, we mistakenly listed someone else during the submission process. As the corresponding author plays a crucial role in academic communication and future collaborations, this error might adversely affect our team's research work.

In light of this, we earnestly request your assistance in correcting the corresponding author information to reflect Professor Haichuan Zhang as the corresponding author.

Received 23 September 2024, Added 25 September 2024